Volume 1 | Number 1 | Jan 2013 | Pages 1–100

Journal of
Materials Chemistry A

Materials for energy and sustainability
www.rsc.org/materialsA

Li⁺

ROYAL SOCIETY
OF CHEMISTRY

ROYAL SOCIETY
OF CHEMISTRY

www.rsc.org/materialsA

Journal Name

Dynamic Article Links ▶

ARTICLE TYPE

Size-controlled SiO$_2$ nanoparticles as scaffold layers in thin-film perovskite solar cells

Sun Hye Hwang, Jongmin Roh, Jungsup Lee, Jeahoon Ryu, Juyoung Yun, and Jyongsik Jang*

Perovskite-based solar cells have received much recent research attention for renewable-energy applications because of their high efficiency and long-term stability. Here, we report perovskite solar cells formed using a scaffold layer
10 **composed of size-controlled SiO$_2$ nanoparticles (NPs). The infiltration of perovskite into the scaffold layer depended strongly on the size of the SiO$_2$ NPs. We investigated the effects of scaffold layers comprised of SiO$_2$ NPs that were 15, 30, 50, 70, and 100 nm in diameter on the properties of the**
15 **perovskite films. The performance of perovskite solar cells based on 50-nm-diameter SiO$_2$ NPs exhibited a current density of J_{sc} = 16.4 mA cm^{-2}, open-circuit voltage of V_{oc} = 1.05 V, and power-conversion efficiency (PCE) of 11.45%, which represents a significant improvement compared with**
20 **perovskite solar cells fabricated using a TiO$_2$ scaffold layer, where J_{sc} = 17.3 mA cm^{-2}, V_{oc} = 0.94 V, and the PCE was 10.29%.**

Solid-state sensitized solar cells have attracted much research interest over the past two decades because of their long-term
25 stability and low costs.[1-4] However, a significant drawback of solid-state sensitized solar cells is the low power-conversion efficiency (PCE), which is typically less than 7.5%.[5] Approaches to improve the photovoltaic performance include the use of additives such as lithium salt bis(trifluoromethane sulfonyl)imide
30 (Li-TFSI) and tris(2-(1H-pyrazol-1-yl)pyridine)cobalt(III) (FK102) with spiro-MeOTAD, which can significantly increase the conductivity of the electrolyte, leading to an increase in the PCE.[5-6] In addition, the use of 4-tert-butylpyridine (tBP) has also been shown to increase of the open-circuit voltage due to a
35 decrease in the charge-carrier recombination rate and the interface-defect density.[7] Furthermore, various hole transporting materials (HTM) such as poly(2,6-(4,4-bis-(2-ethylhexyl)-4*H*-cyclopenta[2,1-b;3,4-b´]dithiophene)-alt-4,7(2,1,3 benzothiadiazole)) (PCPDTBT) and poly(3-hexylthiophene)
40 (P3HT) have been applied to improve the PCE.[8] In spite of these advances, however, achieving a large PCE remains challenging for solid-state sensitized solar cells.

Solid-state perovskite solar cells have been the focus of recent research into solid-state sensitized solar cells because of their
45 superior light-harvesting ability in the solar spectrum, leading to a large PCE.[9-16] The absorption coefficient of perovskite is 1.5 × 10^4 cm^{-1} with a 550-nm-thick scaffold film, which is one order of magnitude larger than that previously reported for solid-state

sensitized solar cells, and is larger than that of ruthenium-based
50 N719 dye or molecular-based organic dyes.[17-18] Thus, effective infiltration, coverage, and coating of perovskite onto the working electrode is highly desirable in order to increase the PCE of solar cells.

Methods to improve the infiltration, coverage, and coating of
55 perovskite onto workings electrodes have been reported. For example, the solubility of the perovskite precursor depends on the solvent used. Dimethyl sulfoxide (DMSO), dimethyl formamide (DMF), and γ-butyrolactone have been reported as solvents for perovskite precursors; DMSO can be used to achieve a high
60 concentration of the precursor with a solubility of up to 60 wt%, which allows for the formation of a dense perovskite film, resulting in a PCE of up to 10.8%.[19] Planar heterojunction
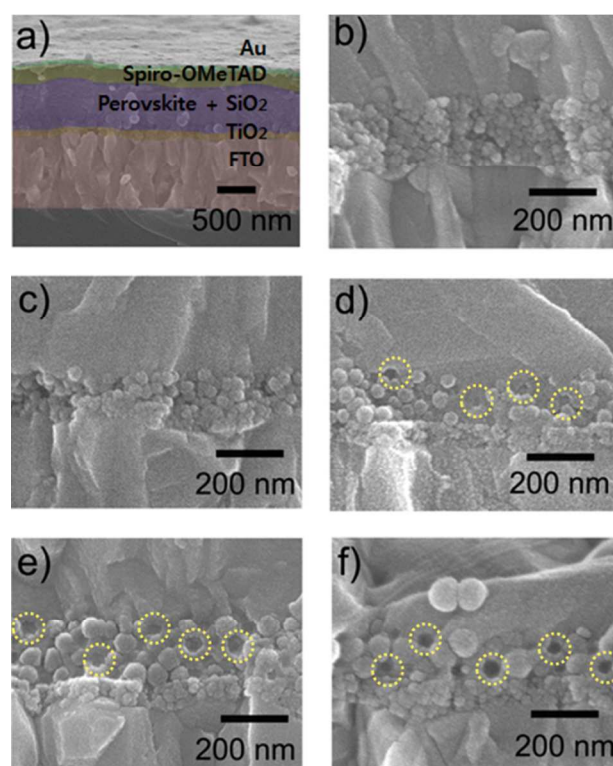

Fig. 1. a) Cross-sectional SEM image of the device structure of perovskite solar cells. b–f) Magnified cross-sectional SEM images of scaffold layers containing SiO$_2$ NPs with diameters of b) 15 nm, c) 30 nm, d) 50 nm, e) 70 nm, and f) 100 nm.

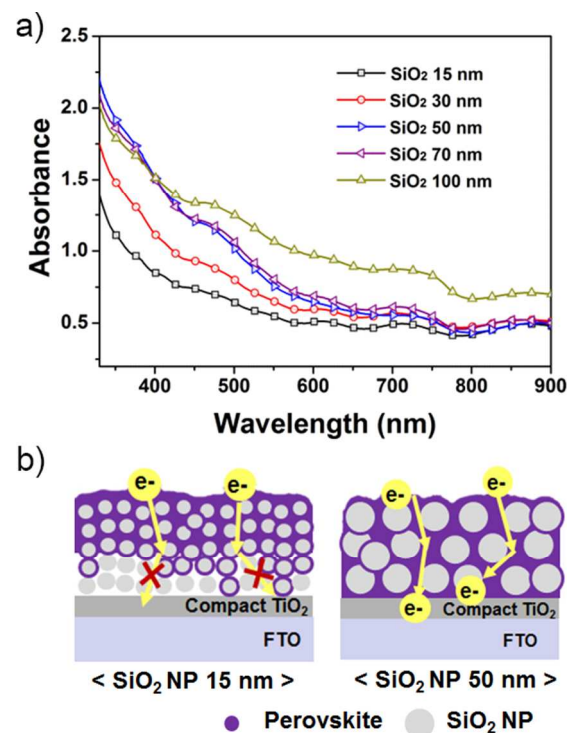Journal of Materials Chemistry A Accepted Manuscript

Fig. 2. a) UV–vis spectra of the perovskite layer containing various diameter SiO₂ NPs b) schematic configuration of perovskite penetration into scaffold layer depending on the size of SiO₂ NPs

perovskite solar cells with full coverage of perovskite incorporating vapour-deposition presented a significant improved PCE of up to 15.4%.[20]

In addition, the morphology of the perovskite film can be controlled by varying the temperature and time. Optimized devices with full surface coverage of perovskite film on working electrodes have exhibited a PCE of up to 11.4%.[21] In addition, various nanomaterials, including TiO_2, Al_2O_3, ZrO_2, and ZnO, have been applied as scaffold layers to increase the perovskite loading on the working electrode of the solar cell.[22-28] In particular, perovskite solar cells with Al_2O_3 or ZrO_2 scaffold layers exhibit a large open-circuit voltage V_{oc} because the conduction band energies of Al_2O_3 and ZrO_2 are higher than that of perovskite, so that electrons cannot readily transfer into the conduction band of either layer.[22, 29] Moreover, infiltration of viscous perovskite solution onto working electrode is also important issue because the scaffold materials cannot transfer the photo-generated electrons to working electrode. The size of nanoparticles composed in scaffold layer could make effect on the infiltration of viscous perovskite solution into working electrode. However, the infiltration depending on nanoparticle size of scaffold layer onto working electrode has not yet been studied. Thus, there is a requirement for optimized designs of scaffold layers, and an associated development of materials.

Here, we report perovskite solar cells formed using size-controlled SiO₂ nanoparticles (NPs) as a scaffold layer. The mono-dispersed SiO₂ NPs could be easily synthesized to get desired size by change the fabrication temperature in compared with other scaffold materials. The infiltration of perovskite into

the scaffold layer was investigated with various diameter SiO₂ NPs. The infiltration was optimized by controlling the size of the SiO₂ NPs. 50-nm-diameter SiO₂ NPs resulted in perovskite solar cells that exhibited the largest PCE, which was 11.45%. This compares favorably with TiO₂-based perovskite solar cells, which had a PCE of 10.29%. To the best of our knowledge, this is the first study into the infiltration of perovskite into a scaffold layer composed of SiO₂ NPs with systematically varied diameters.

SiO₂ NPs with diameters of 15, 30, 50, 70, and 100 nm were synthesized via a sol-gel method.[30-31] The SiO₂ NPs were formed into a scaffold layer by spin coating, and the thickness was adjusted by controlling the number of spin-coating repetitions. A $CH_3NH_3PbI_{3-x}Cl_x$ perovskite absorption and electron transport material was infiltrated into the SiO₂ scaffold layer. 2,2′,7,7′-tetrakis-(N,N-di-p-methoxyphenylamine)9,9′-spirobifluorene (spiro-OMeTAD) was deposited onto the perovskite layer to form a hole transport layer, and Au electrodes were thermally evaporated to make contacts to the devices. The performance of the device was measured under irradiation with AM 1.5G light at an intensity of 100 W cm⁻², with an active device area of 0.09 cm², using a mask. **Fig. 1a** shows a cross-sectional colored field-emission scanning electron microscopy (FE-SEM) image of a device with a SiO₂ scaffold layer. **Fig. 1b–f** show magnified images of the scaffold layer regions in order to investigate the infiltration of perovskite into the SiO₂ scaffold layer. A compact layer, 80 ± 5 nm thick, containing 15 to 20-nm-diameter TiO₂ NPs was located under the SiO₂ scaffold layer. The thickness of the SiO₂ NP scaffold layer was 230 ± 30 nm. In Fig. 1b and 1c, the perovskite did not infiltrate deeply into the mesoporous layer containing the 15- and 30-nm-diameter SiO₂ NPs; however, the scaffold layers formed of larger silica NPs (*i.e.*, 50-, 70-, and 100-nm diameter) exhibited good infiltration of the perovskite into the spaces between the SiO₂ NPs. Fig. 1d–f show holes that originated from some of the SiO₂ NPs leaving the matrix of the mesoporos scaffold layer, indicating that the pore size between the SiO₂ NPs with a diameter of 50 nm or larger was sufficient for perovskite to infiltrate into the scaffold layer. Furthermore, the perovskite appeared to contact with the compact TiO₂ layer. The penetration of perovskite was also investigated using elemental line mapping of the SiO₂ NPs with diameters of 15 and 100 nm
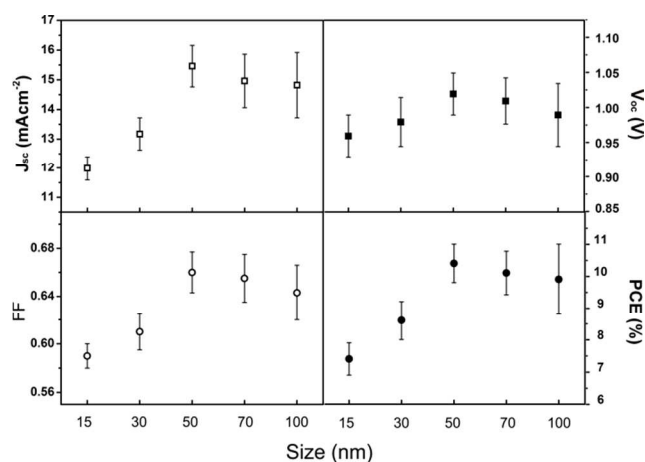

Fig. 3. Dependence of the performance of the perovskite devices on the diameter of the SiO₂ NPs in the scaffold layer.
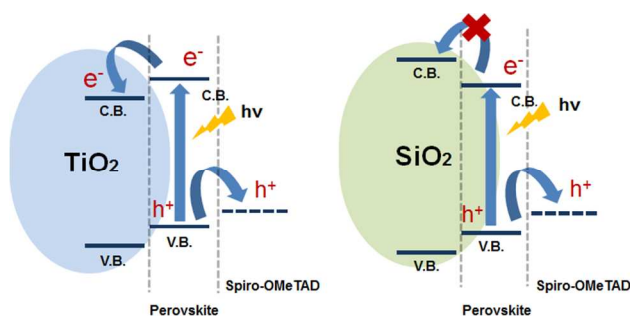
Journal of Materials Chemistry A Accepted Manuscript

Fig. 4. Schematic diagram showing electron and hole transfer in the perovskite solar cells with scaffold layers based on TiO_2 NPs (left) and SiO_2 NPs (right).

using energy dispersive X-ray spectroscopy (EDS) (see Fig. S1). The elements Pb and I were deeply infiltrated for the scaffold layer formed of 100-nm-diameter SiO_2 NPs, but not that formed of 15-nm-diameter SiO_2 NPs. Based on these data, the pore size
5 between SiO_2 NPs strongly influenced the penetration of perovskite into the scaffold layer.

To investigate the absorption of perovskite loaded on the mesoporous layer composed of SiO_2 NPs, the absorption of perovskite was measured using ultraviolet–visible (UV–vis)
10 spectroscopy. The crystallinity of the perovskite layer on the 50-nm-diameter SiO_2 NPs was analyzed using X-ray diffraction (XRD) (see Fig. S2). Interestingly, the optical absorption of the perovskite film increased with the diameter of the silica NPs up to 50 nm, as shown in Fig. 2. This is consistent with the data
15 shown in Fig. 1. It appears that the pore size formed between the SiO_2 NPs with diameters of 15 and 30 nm was too small for the perovskite to infiltrate into the scaffold layer.

Devices formed from scaffold layers with SiO_2 NPs that were 15 and 30 nm in diameter are expected to exhibit relatively small
20 optical absorption. However, devices formed using the scaffold layers with SiO_2 NPs with a diameter for 50 nm or greater can be expected to exhibit much larger optical absorption. The infiltration of perovskite into scaffold layer was illustrated in **Fig. 2b.** In case of SiO_2 NP with size of 15 and 30 nm, the perovskite
25 cannot infiltrate into bottom of scaffold layer, while perovskite well penetrates into scaffold layer comprised of SiO_2 NPs with size of 50, 70, and 100 nm due to the large pore size between SiO_2 NPs. Therefore, the optical absorption of perovskite film composed of SiO_2 NPs with a diameter for 50 nm or greater is
30 much stronger than that of 15 and 30 nm. Interestingly, the absorption of the device with a scaffold layer formed of 100-nm-diameter SiO_2 NPs increased at long wavelengths, which may by related to complex optical scattering effects of the SiO_2 NPs or the perovksite structure. Diffuse reflection spectroscopy (DRS)
35 measurements were carried out to investigate the optical scattering effects with various diameter SiO_2 NPs; none were observed (data not shown). The perovskite structure formed on the SiO_2 NP scaffold layers was also investigated using SEM. The domain size of the perovskite increased with the diameter of the
40 SiO_2 NPs in the mesoporous layer. The domain size of the perovskite deposited on 15-nm-diameter SiO_2 was ~20 μm, whereas the domain size for the 100-nm-diameter SiO_2 NPs was greater than 100 μm (see Fig. S3). Conings *et al.* reported similar

phenomena of perovskite scattering behavior related to the
45 morphology of perovskite layer.[19] The absorption of needle-like perovskite partly decreased the absorption at short wavelengths and increased the absorption at long wavelengths due to the complex scattering behavior. Considering these results, we expect the morphology and optical absorption of the perovskite film will
50 be affected by the size of the SiO_2 NPs.

We fabricated solar cells to investigate the influence of the scaffold layer on the device performance. The thickness of the scaffold layer was maintained constant, as were all other variables, while the diameter of the SiO_2 NPs in the scaffold layer
55 was varied. **Fig. 3** shows the short-circuit photocurrent J_{sc}, open-circuit voltage V_{oc}, fill factor (FF), and the PCE. J_{sc} clearly increased with the diameter of the SiO_2 NPs up to 50 nm, and then decreased slightly with as the diameter increased beyond 50 nm. Based on the UV–vis absorption spectra, the absorption of
60 perovskite film decreased because the perovskite loading was small for SiO_2 NPs with a diameter less than 50 nm, but complex scattering effects occurred as the diameter of the SiO_2 NPs increased above 50 nm. V_{oc} exhibited similar behavior to J_{sc} as a function of the diameter of the SiO_2 NPs. The FF was small in the
65 devices based on the 15- and 30-nm-diameter SiO_2 NPs, which suggests that both the series shunt resistances increased due to less perovskite infiltration into the scaffold layer, resulting in insufficient electron transfer into the compact TiO_2 layer.

The performance metrics shown in Fig. 3 were optimal for the
70 devices formed using scaffold layers composed of 50-nm-diameter SiO_2 NPs. The amount of perovskite loading on the scaffold layer had the most significant effect on the performance of the perovskite solar cell, but the morphology was also important.

75 **Fig. 4** shows a schematic diagram illustrating the energy levels of the conduction and valence bands in TiO_2, SiO_2, and perovskite. Importantly, the conduction band energy of TiO_2 is lower than that of perovskite, whereas the conduction band energy of SiO_2 is higher than that of perovskite. The amorphous
80 SiO_2 NPs are insulators with a wide band gap of approximately 9–11 eV.[32-33] When a photon is absorbed in the perovskite layer, in the devices with a scaffold layer formed of TiO_2 NPs, the photo-generated electron may transfer from perovskite to TiO_2; however, in the devices with a scaffold layer formed of SiO_2 NPs,
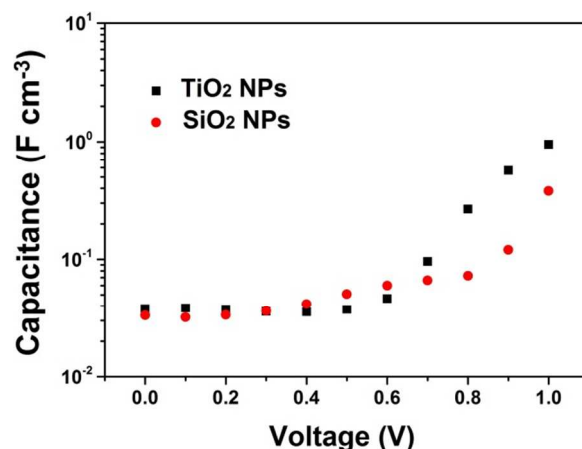

Fig. 5. Capacitance of the TiO_2- and SiO_2-based perovskite solar cells as a function of the applied voltage (under dark conditions).
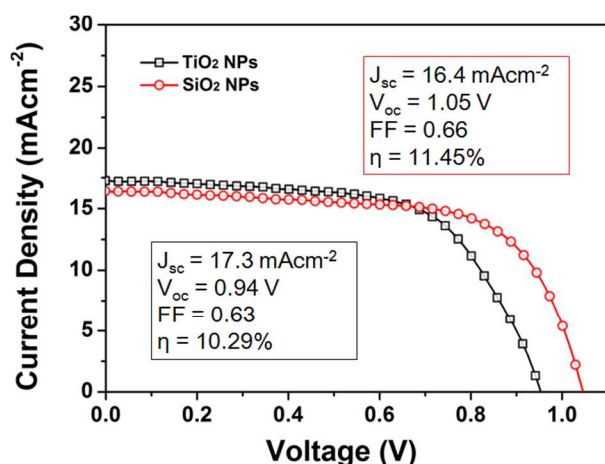
Fig. 6. Current density–voltage (J–V) characteristics of the perovskite solar cells with scaffold layers formed of TiO$_2$ and SiO$_2$ NPs under illumination with an AM 1.5G 100 W cm^{-2} light source.

electrons cannot transfer to the SiO$_2$ NPs. For this reason, TiO$_2$ forms an electron transport layer in devices with TiO$_2$-based scaffolds, whereas perovskite forms an electron-transport layer in devices with SiO$_2$-based scaffolds. In both devices, photo-generated holes may transfer from the valence band of perovskite into the spiro-OMeTAD, which forms the hole-transport layer. In this respect, the behavior of SiO$_2$ is similar that of Al$_2$O$_3$ and ZrO$_2$ NPs, as has been reported previously.[22, 29]

The capacitance of solar cells containing TiO$_2$ and SiO$_2$ NPs was investigated without illumination. **Fig. 5a** shows the capacitance of perovskite solar cells as a function of the applied voltage. The bias dependence of the capacitance of both the TiO$_2$- and SiO$_2$-based perovskite solar cells exhibited similar trends, whereby the capacitance increased as a function of the applied bias V_{app}. At low applied biases (*i.e.*, $V_{app} < 0.6$ V), similar behavior was observed for both perovskite solar cells. At larger biases (*i.e.*, $V_{app} > 0.6$ V), the capacitance increased exponentially, and the capacitance of the SiO$_2$-based solar cells was lower that of the TiO$_2$-based devices. Kim *et al.* reported that at biases greater than approximately 0.6 to 0.7 V, the capacitance of ZrO$_2$-based perovskite solar cells increased exponentially because of charge accumulation in the compact TiO$_2$ layer and the perovskite, but not in the ZrO$_2$. Furthermore, the capacitance of the TiO$_2$ electrode is greater than that of the ZrO$_2$ electrode due to the larger volume of TiO$_2$ compared with the ZrO$_2$ electrode.[34] The SiO$_2$-based perovskite solar cells have a

similar configuration to the ZrO$_2$-based perovskite solar cells described in Ref. 32. Thus, the SiO$_2$-based devices reported here appear to exhibit a similar bias dependence of the capacitance.

The current density–voltage (J–V) characteristics of perovskite solar cells with TiO$_2$ and SiO$_2$ scaffold layers were measured using a mask under illumination with an AM 1.5G light source with a power density of 100 W cm^{-2}. The thickness of the scaffold layer containing TiO$_2$ and SiO$_2$ was 230 ± 30 nm. In Fig. 6, the perovskite solar cells with a TiO$_2$ scaffold layer exhibited $J_{sc} = 17.3$ mA cm^{-2}, which is larger than the current density of the perovskite solar cells with a SiO$_2$ scaffold layer, where $J_{sc} = 16.4$ mA cm^{-2}. The larger current density may result from the

difference in the conduction band energy of TiO$_2$ and SiO$_2$. The conduction band energy of TiO$_2$ is lower than that of perovskite, resulting in electron transfer from pervoskite into the TiO$_2$. Suarez et al. demonstrate that the recombination rate of TiO$_2$ and Al$_2$O$_3$ plays important role in the open-circuit voltage, V_{oc}.[35] Marchioro *et al.* also reported that the charge-carrier recombination rate of TiO$_2$ is significantly slower than that of Al$_2$O$_3$ films.[33] A slower charge-carrier recombination rate is related to the larger V_{oc}, which may explain the larger V_{oc} in the TiO$_2$-based solar cells compared with the SiO$_2$-based devices. In addition, the TiO$_2$- and SiO$_2$-based perovskite solar cells have different operating principles. When light is absorbed in the TiO$_2$-based perovskite solar cells, photogenerated electrons transfer into the TiO$_2$. In contrast, in the SiO$_2$-based devices, photogenerated electrons remain in the perovskite. It has effect on the V_{oc}. To further investigate the electron injection into TiO$_2$ and SiO$_2$ NPs, we measured the photoluminescence (PL) in **Fig. S4**. The PL quantum yield of the TiO$_2$/perovskite solar cell is greatly reduced compared with SiO$_2$/perovskite solar cell. It is considered that the photogenerated electrons in the perovskite are quenched by electron injection into TiO$_2$. As a result, the open-circuit voltage is larger: 10.5 V for the SiO$_2$-based devices compared with 0.94 V for the TiO$_2$-based devices. The PCE of the SiO$_2$-based solar cell was 11.45%, whereas that of the TiO$_2$-based device was 10.29%.

Conclusions

We have described the use of size-controlled SiO$_2$ NPs as a scaffold layer in perovskite-based solar cells. The size of the pores formed between SiO$_2$ NPs depended on the diameter of the NPs, and this was found to affect the infiltration of perovskite into the scaffold layer. SiO$_2$ NPs with a diameter of 50 nm resulted in efficient infiltration of perovskite while maintaining favorable optical properties, resulting in optimum performance of the solar cells. Furthermore, both SiO$_2$-based and TiO$_2$-based perovskite solar cells exhibited a similar bias dependence of the capacitance. The open-circuit voltage of the SiO$_2$-based solar cells was larger than that of the TiO$_2$-based devices, which led to a larger PCE of 11.45% for the SiO$_2$-based solar cells, compared with 10.29% for the TiO$_2$-based solar cells.

Acknowledgment

Notes and references

World Class University (WCU) program of Chemical Convergence for Energy & Environment (C$_2$E$_2$), School of Chemical and Biological Engineering, College of Engineering, Seoul National University, 599 Gwanangno, Gwanakgu, Seoul, 151-742 (Korea) Fax: +82-2-888-1604; Tel.: +82-2-880-7069; E-mail: jsjang@plaza.snu.ac.kr

1   U. Bach, D. Lupo, P. Comte, J. E. Moser, F. Weissörtel, J. Salbeck, H. Spreitzer and M. Grätzel, *Nature*, 1998, **395**, 583-585.
2   D. P. Hagberg, J. H. Yum, H. Lee, F. De Angelis, T. Marinado, K. M. Karlsson, R. Humphry-Baker, L. Sun, A. Hagfeldt, M. Grätzel and M.

K. Nazeeruddin, *J. Am. Chem. Soc.*, 2008, **130**, 6259-6266.

3 J. Krüger, R. Plass, L. Cevey, M. Piccirelli, M. Grätzel and U. Bach, *Appl. Phys. Lett.*, 2001, **79**, 2085-2087.

4 W. M. Campbell, K. W. Jolley, P. Wagner, K. Wagner, P. J. Walsh, K. C. Gordon, L. Schmidt-Mende, M. K. Nazeeruddin, Q. Wang, M. Grätzel and D. L. Officer, *Journal of Physical Chemistry C*, 2007, **111**, 11760-11762.

5 J. Burschka, A. Dualeh, F. Kessler, E. Baranoff, N. L. Cevey-Ha, C. Yi, M. K. Nazeeruddin and M. Grätzel, *J. Am. Chem. Soc.*, 2011, **133**, 18042-18045.

6 A. Abate, T. Leijtens, S. Pathak, J. Teuscher, R. Avolio, M. E. Errico, J. Kirkpatrik, J. M. Ball, P. Docampo, I. McPherson and H. J. Snaith, *PCCP*, 2013, **15**, 2572-2579.

7 G. Boschloo, L. Häggman and A. Hagfeldt, *J. Phys. Chem. B*, 2006, **110**, 13144-13150.

8 Y. C. Choi, D. U. Lee, J. H. Noh, E. K. Kim and S. I. Seok, *Adv. Funct. Mater.*, 2014, **24**, 3587-3592.

9 K. Wojciechowski, M. Saliba, T. Leijtens, A. Abate and H. J. Snaith, *Energy Environ. Sci.*, 2014, **7**, 1142-1147.

10 N. G. Park, *Journal of Physical Chemistry Letters*, 2013, **4**, 2423-2429.

11 W. Zhang, M. Saliba, S. D. Stranks, Y. Sun, X. Shi, U. Wiesner and H. J. Snaith, *Nano Lett.*, 2013, **13**, 4505-4510.

12 J. Burschka, N. Pellet, S. J. Moon, R. Humphry-Baker, P. Gao, M. K. Nazeeruddin and M. Grätzel, *Nature*, 2013, **499**, 316-319.

13 G. E. Eperon, V. M. Burlakov, A. Goriely and H. J. Snaith, *ACS Nano*, 2014, **8**, 591-598.

14 A. Abrusci, S. D. Stranks, P. Docampo, H. L. Yip, A. K. Y. Jen and H. J. Snaith, *Nano Lett.*, 2013, **13**, 3124-3128.

15 B. Cai, Y. Xing, Z. Yang, W. H. Zhang and J. Qiu, *Energy Environ. Sci.*, 2013, **6**, 1480-1485.

16 T. Leijtens, G. E. Eperon, S. Pathak, A. Abate, M. M. Lee and H. J. Snaith, *Nature Communications*, 2013, **4**.

17 H. S. Kim, J. W. Lee, N. Yantara, P. P. Boix, S. A. Kulkarni, S. Mhaisalkar, M. Grätzel and N. G. Park, *Nano Lett.*, 2013, **13**, 2412-2417.

18 J. H. Im, C. R. Lee, J. W. Lee, S. W. Park and N. G. Park, *Nanoscale*, 2011, **3**, 4088-4093.

19 B. Conings, L. Baeten, C. De Dobbelaere, J. D'Haen, J. Manca and H. G. Boyen, *Adv. Mater.*, 2014, **26**, 2041-2046.

20 M. Liu, M. B. Johnston and H. J. Snaith, *Nature*, 2013, **501**, 395-398.

21 G. E. Eperon, V. M. Burlakov, P. Docampo, A. Goriely and H. J. Snaith, *Adv. Funct. Mater.*, 2014, **24**, 151-157.

22 M. M. Lee, J. Teuscher, T. Miyasaka, T. N. Murakami and H. J. Snaith, *Science*, 2012, **338**, 643-647.

23 H. S. Kim, C. R. Lee, J. H. Im, K. B. Lee, T. Moehl, A. Marchioro, S. J. Moon, R. Humphry-Baker, J. H. Yum, J. E. Moser, M. Grätzel and N. G. Park, *Scientific Reports*, 2012, **2**.

24 A. Kojima, K. Teshima, Y. Shirai and T. Miyasaka, *J. Am. Chem. Soc.*, 2009, **131**, 6050-6051.

25 J. H. Noh, S. H. Im, J. H. Heo, T. N. Mandal and S. I. Seok, *Nano Lett.*, 2013, **13**, 1764-1769.

26 J. M. Ball, M. M. Lee, A. Hey and H. J. Snaith, *Energy Environ. Sci.*, 2013, **6**, 1739-1743.

27 M. H. Kumar, N. Yantara, S. Dharani, M. Graetzel, S. Mhaisalkar, P. P. Boix and N. Mathews, *Chem. Commun.*, 2013, **49**, 11089-11091.

28 D. Bi, G. Boschloo, S. Schwarzmüller, L. Yang, E. M. J. Johansson and A. Hagfeldt, *Nanoscale*, 2013, **5**, 11686-11691.

29 D. Bi, S. J. Moon, L. Häggman, G. Boschloo, L. Yang, E. M. J. Johansson, M. K. Nazeeruddin, M. Grätzel and A. Hagfeldt, *RSC Advances*, 2013, **3**, 18762-18766.

30 W. Stöber, A. Fink and E. Bohn, *Journal of Colloid And Interface Science*, 1968, **26**, 62-69.

31 Z. H. Chen, C. Kim, X. B. Zeng, S. H. Hwang, J. Jang and G. Ungar, *Langmuir*, 2012, **28**, 15350-15361.

32 T. H. DiStefano and D. E. Eastman, *Solid State Communications*, 1971, **9**, 2259-2261.

33 E. Vella, F. Messina, M. Cannas and R. Boscaino, *Physical Review B - Condensed Matter and Materials Physics*, 2011, **83**.

34 H. S. Kim, I. Mora-Sero, V. Gonzalez-Pedro, F. Fabregat-Santiago, E. J. Juarez-Perez, N. G. Park and J. Bisquert, *Nature Communications*, 2013, **4**.

35 B. Suarez, V. Gonzalez-Pedro, T. S. Ripolles, R. S. Sanchez, L. Otero and I. Mora-Sero, *Journal of Physical Chemistry Letters*, 2014, **5**, 1628-1635.

Graphical Abstract
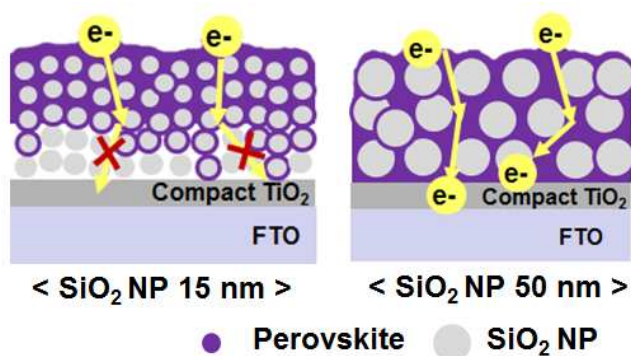
The effects of scaffold layers composed of SiO_2 NPs with diameters of 15, 30, 50, 70, and 100 nm were investigated on the properties of the perovskite film. Among the various size of SiO_2 NPs, the performance of 50-nm-diameter SiO_2 NPs based perovskite solar cell presented high power-conversion efficiency (PCE) of 11.45%.